J Neurophysiol 96: 834–845, 2006.
First published May 17, 2006; doi:10.1152/jn.01079.2005.

Electrophysiological Classification of Somatostatin-Positive Interneurons in Mouse Sensorimotor Cortex

Brian Halabisky, Fran Shen, John R. Huguenard, and David A. Prince
Department of Neurology and Neurological Sciences, Stanford University School of Medicine, Stanford, California

Submitted 12 October 2005; accepted in final form 30 April 2006

Halabisky, Brian, Fran Shen, John R. Huguenard, and David A. Prince. Electrophysiological classification of somatostatin-positive interneurons in mouse sensorimotor cortex. *J Neurophysiol* 96: 834–845, 2006. First published May 17, 2006; doi:10.1152/jn.01079.2005. Classification of inhibitory interneurons is critical in determining their role in normal information processing and pathophysiological conditions such as epilepsy. Classification schemes have relied on morphological, physiological, biochemical, and molecular criteria; and clear correlations have been demonstrated between firing patterns and cellular markers such as neuropeptides and calcium-binding proteins. This molecular diversity has allowed generation of transgenic mouse strains in which GFP expression is linked to the expression of one of these markers and presumably a single subtype of neuron. In the GIN mouse (E*G*FP-expressing *I*nhibitory *N*eurons), a subpopulation of somatostatin-containing interneurons in the hippocampus and neocortex is labeled with enhanced green fluorescent protein (EGFP). To optimize the use of the GIN mouse, it is critical to know whether the population of somatostatin–EGFP-expressing interneurons is homogeneous. We performed unsupervised cluster analysis on 46 EGFP-expressing interneurons, based on data obtained from whole cell patch-clamp recordings. Cells were classified according to a number of electrophysiological variables related to spontaneous excitatory postsynaptic currents (sEPSCs), firing behavior, and intrinsic membrane properties. EGFP-expressing interneurons were heterogeneous and at least four subgroups could be distinguished. In addition, multiple discriminant analysis was applied to data collected during whole cell recordings to develop an algorithm for predicting the group membership of newly encountered EGFP-expressing interneurons. Our data are consistent with a heterogeneous population of neurons based on electrophysiological properties and indicate that EGFP expression in the GIN mouse is not restricted to a single class of somatostatin-positive interneuron.

INTRODUCTION

In the neocortex, 70–80% of neurons are excitatory pyramidal cells (DeFelipe and Farinas 1992; Peters and Sethares 1991) that, although having diverse anatomical, physiological, and molecular properties (DeFelipe and Farinas 1992), do not show the same degree of heterogeneity as that in the remaining 20–30% of what are mostly inhibitory interneurons. Inhibitory interneurons use γ-aminobutyric acid (GABA) as their transmitter with their axonal and dendritic arbors restricted to the neocortex (Letinic et al. 2002). Subgroups of these interneurons are distinguishable on the bases of their location; microanatomical features, including dendritic arborizations and axonal projections; expression of specific cellular markers; and neurophysiological properties (Bacci et al. 2003a,b; Cauli et al. 1997; DeFelipe 1993, 2002; Gupta et al. 2000; Kawaguchi and Kubota 1997; Somogyi et al. 1998; Thomson and Deuchars 1994). However, the classification of GABAergic cortical cells into distinct subgroups is complicated by the amount of overlap among these characteristics (Maccaferri and Lacaille 2003; Markram et al. 2004; Mott and Dingledine 2003).

Somatic, dendritic, or axonal morphologies do not reliably define the interneuronal subtype, although subgroups of interneurons can be differentiated on the basis of their intra- and intercolumnar axonal projections that selectively target subdomains of postsynaptic cells, including axons, somata, proximal dendrites, and dendritic tufts (DeFelipe 1997; Somogyi et al. 1998). To facilitate the study of GABAergic neurons, a transgenic mouse line was created that selectively expressed the "enhanced" derivative of green fluorescent protein (EGFP) in subpopulations of somatostatin (SST)-containing interneurons (Oliva Jr. et al. 2000). SST-expressing interneurons in neocortex ("SST interneurons" or "SST cells" below) have heterogeneous firing patterns and are classified as regular or burst spiking (Kawaguchi and Kubota 1996). There is also heterogeneous expression of calbindin D_{28k} (CB) in populations of SST interneurons (Cauli et al. 1997; Kawaguchi and Kubota 1996). It is not known, however, whether EGFP expression in the GIN (E*G*FP-expressing *i*nhibitory *n*eurons) mouse is restricted to a particular subtype of SST interneuron. Detailed information about the characteristics of EGFP-expressing interneurons is required if the transgenic GIN mouse is to be useful for studying the function of SST interneurons in cortical circuits. For example, to determine the role of these labeled cells in physiological or pathophysiological processes, it is important to determine whether they represent a uniform or heterogeneous population of interneurons.

We addressed the question of hetero- or homogeneity of SST/EGFP-expressing interneurons by performing unsupervised cluster analysis of electrophysiological data obtained with whole cell patch-clamp recordings. Cluster analysis allows the classification of objects without a biased a priori scheme based on more casual grouping of data observations. On the basis of electrophysiological parameters, we found that the EGFP-expressing population of neocortical interneurons is heterogeneous, containing at least four distinct groups that likely play different roles in neocortical circuits and information processing. Multiple discriminant analysis, which is used to weight variables so they can be used to classify objects into categories, was also applied to the groups to develop an algorithm used to prospectively classify a given EGFP-expressing interneuron.

Address for reprint requests and other correspondence: D. A. Prince, Department of Neurology and Neurological Sciences, Stanford University School of Medicine, Stanford, CA 94305-5122 (E-mail: daprince@stanford.edu).

The costs of publication of this article were defrayed in part by the payment of page charges. The article must therefore be hereby marked "*advertisement*" in accordance with 18 U.S.C. Section 1734 solely to indicate this fact.

METHODS

Immunohistochemistry

All experiments were carried out according to protocols approved by the Stanford Institutional Animal Care and Use Committee. Three GIN mice [Oliva Jr. et al. 2000; Strain FVB-TgN(GadGFP)45704Swn, Jackson Laboratories] were anesthetized with pentobarbital [50 mg/kg, administered intraperitoneally (ip)] and perfused through the heart with saline followed by 4% paraformaldehyde in 0.1 M phosphate buffer (Sigma, St. Louis, MO), pH 7.4. The brains were removed and postfixed in 4% phosphate-buffered paraformaldehyde at 4°C overnight and then cryoprotected with 30% sucrose buffer and frozen on dry ice. Coronal sections (40 μm) were cut with a cryostat (Microm HM 500; Heidelberg, Germany) and nonadjacent representative sections from anterior through posterior sensorimotor cortex were selected and examined under fluorescence to ensure the existence of EGFP cells. Sections were then processed for immunolabeling with antibodies against GFP, SST, parvalbumin (PV), calbindin D_{28k} (CB), and calretinin (CR), using a two-stage immunofluorescent labeling procedure. Free-floating sections were rinsed twice in PBS buffer followed by 50% alcohol. Nonspecific binding was blocked by incubating the sections in 10% normal goat serum. To detect the particular proteins, sections were then exposed to the following primary antisera at 4°C overnight: EGFP (1:1,000; Molecular Probes, Eugene, OR), SST (1:500; Peninsula Laboratories, San Carlos, CA), PV (1:2,000), and CB (1:4,000; gift from K. Baimbridge, University of British Columbia), and CR (1:500; Chemicon, Temecula, CA). They were then treated for 2 h at room temperature with secondary antibody conjugated to fluorescein and/or indocarbocyanine (FITC and/or Cy3, 1:200; Jackson ImmunoResearch Lab, West Grove, PA), air dried, and mounted on microscope slides with Vectashield mounting medium (Vector Laboratories, Burlingame, CA).

Cell counts

Immunofluorescence-labeled sections cut through sensorimotor cortex were examined under a fluorescence microscope (Nikon Eclipse E800) equipped with an AxioCam digital color camera (Carl Zeiss MicroImaging, Thornwood, NY). Images were captured from both hemispheres at distances between 0.5 and 3 mm from the midline using dual-channel scanning without altering the focal plane. Co-localization was determined by examining EGFP-expressing interneurons for SST, PV, CB, or CR immunoreactivity (IR). Cell counts were performed from at least three nonadjacent sections per animal in a 1.4-mm-long counting window extending through layers I to VI. A confocal laser scanning microscope (Zeiss LSM 150) was also used to obtain images of co-localized IR.

Slice preparation

Twenty-two GIN mice, 28 to 35 days old, were used for in vitro recordings. Techniques for preparing and maintaining brain slices in vitro were as previously described (Li and Prince 2002). Animals were deeply anesthetized with sodium pentobarbital (55 mg/kg ip), decapitated, and the brains rapidly removed and placed in cold (4°C) oxygenated cutting solution containing (in mM): 2.5 KCl, 1.25 $NaPO_4$, 10 $MgSO_4$, 0.5 $CaCl_2$, 26 $NaHCO_3$, 11 glucose, and 234 sucrose. A block of brain containing sensorimotor cortex (S1; Franklin and Paxinos 1997) was fastened to the stage of a D.S.K. vibratome (Dosaka, Kyoto, Japan) with cyanoacrylate (Krazy Glue) and 300-μm coronal slices were cut in the preceding solution. Slices were then incubated for ≥30 min in standard artificial cerebrospinal fluid (ACSF; 30°C) that contained (in mM): 2.5 KCl, 126 NaCl, 10 glucose, 1.25 NaH_2PO_4, 1 $MgSO_4$, 2 $CaCl_2$, and 26 $NaHCO_3$ (pH ≈ 7.4 when gassed with a mixture of 95% O_2-5% CO_2), after which they were maintained at room temperature. Single slices were transferred to a submerged recording chamber where they were maintained at 30°C and perfused at a rate of 2 mL/min.

Cell morphology

EGFP-expressing interneurons were classified into morphological groups based on fluorescent images obtained from live slices in the submerged recording chamber before patch-clamp recordings. Cells that had three or more dendrites distributed evenly about the soma circumference were classified as multipolar (Fig. 2*A*). Bipolar cells had fusiform somata with the long-axis diameter more than twice that of the orthogonal axis and a single dendrite arising from each pole (Fig. 2*B*). Unipolar cells had a large single dendrite with two or more small dendrites opposed (Fig. 2*C*). Composites of images taken at multiple focal planes were obtained using cooled CCD cameras (Fig. 2*A*: Cooke Sensicam QE; Fig. 2, *B* and *C*: Photometrics Cascade 512f).

Recordings

Recordings were made from individual EGFP-expressing interneurons located in cortical layers II and III, identified under fluorescent and infrared differential interference contrast (IR-DIC) video microscopy with a Zeiss Axioskop 2 FS plus microscope. Patch pipettes (4–6 MΩ) were pulled from borosilicate glass (WPI, Sarasota, FL) and filled with (in mM) 5 KCl, 135 K-gluconate, 2 NaCl, 10 HEPES, 4 EGTA, 4 MgATP, and 0.3 Na_3GTP (pH ≈ 7.2; 285 mosmol). Liquid junction potentials were determined using the junction potential calculator in Clampex 9.0 software and corrected during data analysis. Electrophysiological data for analysis were obtained from interneurons that had a resting membrane potential (V_R) more negative than −50 mV, action potentials (APs) overshooting beyond +10 mV, dendritic trees that visually appeared intact with no beading (example of beaded dendrite can be seen in Fig. 2*A*, *right*), and input resistance (R_{in}) >100 MΩ.

Electrophysiological analysis

Eleven electrophysiological parameters were determined for each cell. Spontaneous excitatory postsynaptic currents (sEPSCs) were recorded for 5 min in voltage clamp. From these 5-min epochs, average sEPSC *1*) peak amplitude, *2*) 10/90% rise time, *3*) 90/10% decay time, and *4*) frequency were determined. Current-clamp recordings were used to determine *5*) AP half-width (APHW), *6*) AP afterhyperpolarization (AHP) shape index, *7*) frequency adaptation of AP trains evoked by depolarizing current pulses, *8*) steady-state firing frequency (SSFF), *9*) sag conductance (G_S), *10*) membrane time constant (τ_m), and *11*) input resistance (R_{in}).

Afterpotentials that followed action potentials were biphasic, with short- and long-latency components in most cells. An AP–AHP shape index was calculated as the difference in mean membrane potential between one window at 4.5 ± 1.5 ms after the maximal primary AHP peak (the first negative peak after the AP) and another window at 21.2 ± 4.0 ms after the primary AHP. These windows were determined from the average (±SD) times at which the primary and secondary AHP local maxima and minima voltage peaks occurred (e.g., see Fig. 4*C1*, arrows). The instantaneous frequency of APs in trains evoked by 125-pA, 500-ms depolarizing current pulses was fitted with a single exponential decay ($y = y_0 + Ae^{-x/\tau}$, where y_0 is the y offset or asymptote, A is amplitude, τ is decay time constant, and x is time); τ is a measure of frequency adaptation and y_0 is a measure of SSFF (see Fig. 4*B*). The slope of the frequency–current (*f–I*) relationship approached zero with currents ≥125 pA (data not shown), indicating that the *f–I* relationship saturated near 125 pA. Parameters describing linear fits of the *f–I* relationship in this saturated range (terminal *f–I* slope) are shown in Table 2 and demonstrate that there were no significant differences between any of the groups. Of the 46 cells only four (one from

groups 1 and 4; two from group 3) had slopes significantly different from 0 (1 at $P < 0.01$; 3 at $P < 0.05$).

Cellular input resistance was also not significantly different between cell groups (Table 2), thus justifying the use of a standard current intensity of 125 pA for measuring frequency adaptation and SSFF for all cells. Current pulses were delivered from the cell's resting membrane potential (RMP, with no holding current applied); RMPs were not significantly different between cell groups (Table 2). Sag conductance was measured using a parallel resistor model in which $G_S = R_T^{-1} - R_{in}^{-1}$, where G_S is the membrane conductance activated on hyperpolarization, R_T is the total membrane resistance when the sag conductance is active, and R_{in} is the membrane resistance without the sag conductance active. R_T was measured as the slope of the linear portion of a current–voltage (*I–V*) plot, where *V* was determined as the average voltage of a 5-ms window at the end of a 500-ms hyperpolarizing current pulse and R_{in} as the slope of the linear portion of an *I–V* plot, where *V* was determined near rest as the maximal negative potential during the 500-ms hyperpolarizing pulse (see Fig. 4*A*, *insets*). τ_m was determined by fitting voltage responses to hyperpolarizing current pulses with a standard single-exponential decay ($y = y_0 + Ae^{-t}/\tau_m$, where y_0 is the y offset or asymptote, A is amplitude, τ_m is decay time constant, and t is time). Only responses in which there was no sag in the membrane voltage response were analyzed. Series resistance (R_S) was calculated for all cells based on the amplitude of the capacitive current in response to a 10-mV step.

Statistical analysis

To classify the cells, unsupervised cluster analysis (Ward's method; Ward 1963) using statistical software on a microcomputer was performed (SPSS 12.0, SPSS, Chicago, IL; custom program written in Origin 7.0, OriginLabs, Northampton, MA). Briefly, this analysis consists of plotting individual objects (cells) in multidimensional space, where each axis represents an individual parameter. The two cells spatially closest to each other are grouped together in the first stage of processing to form a new individual object. At each subsequent stage the nearest objects are grouped together, thus reducing the number of objects by one until the last stage (the $n - 1^{th}$ stage, where *n* is the number of total objects) of processing, when there is a single group consisting of all objects. Ward's method determines the "closeness" of objects by finding mergers that give the least possible increase of the within-group error sum of squares (ESS). The final number of clusters was suggested by the Thorndike procedure (Thorndike 1953), where large distances between the centroids of joined groups at a particular stage relative to other stages suggest there are significant differences between the groups (see Fig. 3*A*, *inset*). Average within-cluster distance shown in the dendrograms of Fig. 3 represents the squared Euclidean distance between the centroids of the merged clusters.

Parameters were chosen based on their lack of linear correlation with each other and the presence of multimodality within the parameter. Further analysis was done using multiple discriminant analysis (MDA) to determine the variables most valuable in predicting group membership. The cluster analysis was then reperformed using these strongly discriminating variables: sEPSC peak amplitude, rise time, and decay time; steady-state firing frequency; sag conductance; τ_m; and AP–AHP shape. MDA was also used to develop discriminant functions used in predicting group membership of EGFP cells from GIN mice. Briefly this analysis consists of a linear combination of variables by assigning weights to each of the parameters to maximize the between-group variance relative to the within-group variance for each discriminant function. The discriminant functions take the following form

$$Z_{jk} = c + W_1X_{1k} + W_2X_{2k} + \cdots + W_nX_{nk}$$

where Z_{jk} is the discriminant *Z* score of discriminant function *j* for object *k*, *c* is the intercept, W_i is the discriminant weight for independent variable *i*, and X_{ik} is the independent variable *i* for object *k*.

The number of discriminant functions generated is always g − 1 (where g = number of groups being discriminated), although some functions may offer relatively little discriminating power compared with others.

RESULTS

EGFP neocortical cells are SST-containing GABAergic interneurons most prominent in layers II–IV

Numerous EGFP-expressing neurons were found throughout somatosensory cortex (Fig. 1). Somata were restricted almost exclusively to layers II–IV and upper layer V, and the vast majority of processes containing EGFP were also restricted to these laminae, leading to an increased overall fluorescence in the neuropil. EGFP was present throughout the cytoplasm of expressing neurons. In fixed preparations, the overwhelming majority of EGFP-expressing neurons were intensely fluorescent, making the dendrites readily visible and traceable to their terminations. Axons could also be visualized and followed for hundreds of micrometers from their parent somata. Also, as previously reported (Oliva Jr. et al. 2000), numerous EGFP-expressing neurons of the neocortex are sparsely to moderately spiny. Intensely fluorescent EGFP-containing cells with prominent somata and dendritic arbors could also be seen in live slices maintained in vitro (Fig. 2).

The morphologies of EGFP-expressing neurons are quite diverse. Despite this, three general morphological subtypes can be distinguished, as described in METHODS: *1*) multipolar neurons, which are most prevalent (Fig. 2*A*); *2*) cells with long fusiform somata and a bipolar dendritic configuration (Fig. 2*B*), and *3*) a group having one prominent dendrite oriented

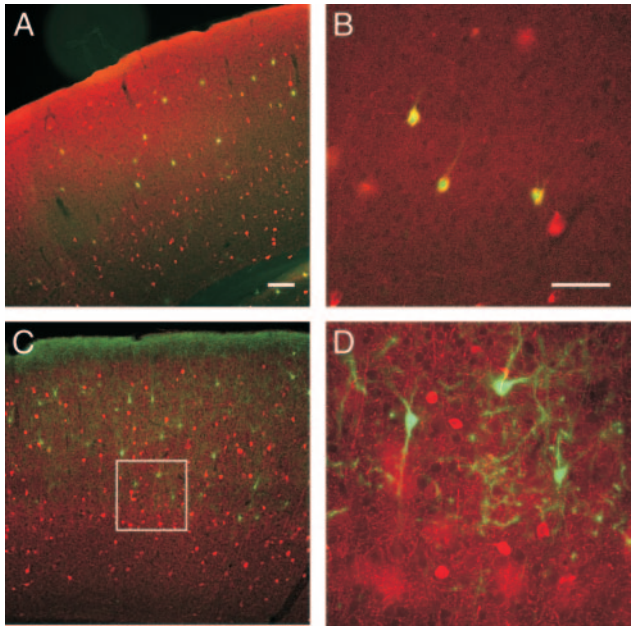

FIG. 1. Enhanced green fluorescent protein (EGFP) is co-localized with somatostatin (SST) but not with parvalbumin (PV) in GIN (*E*GFP-expressing *i*nhibitory *n*eurons) mice. *A*: superimposed epifluorescence visualization of native EGFP fluorescence with SST immunoreactivity (EGFP, green; SST, red). *B*: higher-magnification image showing some co-localization of EGFP and SST immunoreactivity. *C*: superimposed epifluorescence visualization of EGFP immunoreactivity and PV immunoreactivity (EGFP, green; PV, red). *D*: *inset* in *C* enlarged, showing lack of overlap. Scale bar in *A* for *A* and *C*: 100 μm; in *B* for *B* and *D*: 50 μm.

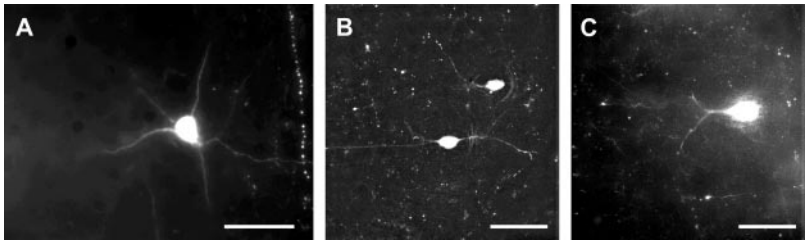

FIG. 2. Images of EGFP-expressing cells in live brain slices captured with a cooled CCD camera. These are composited from images taken at several focal planes to capture more of the dendritic tree. *A*: multipolar cell with dendrites extending from the soma in multiple opposing directions. A beaded dendrite can be seen at the *right*. *B*: bipolar cell with dendrites extending from opposite poles before branching. *C*: unipolar cell with a single large dendrite extending toward the pial surface. In each panel the pia is to the *left*. Scale bars are 50 μm.

toward the pial surface and forming multiple branches extending into layer I (Fig. 2*C*).

Cellular markers in EGFP-expressing interneurons in neocortex

Although it was previously shown that EGFP-expressing interneurons in GIN mice coexpress SST (Oliva Jr. et al. 2000), we performed immunohistochemistry on fixed sections of GIN mouse somatosensory cortex to confirm this finding. Results showed that nearly all, if not every, EGFP-expressing interneuron coexpressed SST (Table 1, Fig. 1, *A–C*). However, as previously shown (Oliva Jr. et al. 2000), not all SST interneurons were EGFP expressing, indicating that the EGFP-expressing interneurons are a subset of SST-containing interneurons (Fig. 1*A*). SST-containing neurons are generally thought to be low-threshold spiking [LTS, also known as burst spiking nonpyramidal (BSNP)] or regular-spiking nonpyramidal (RSNP) cells that differ from fast-spiking (FS) interneurons in terms of their electrophysiological characteristics. Also FS interneurons contain the calcium-binding protein parvalbumin (PV), whereas LTS cells do not (Cauli et al. 1997; Kawaguchi and Kondo 2002). To confirm that the EGFP-expressing interneurons were distinct from FS cells, we assessed PV immunoreactivity in neocortical sections from GIN mouse and found that PV and EGFP occurred in nonoverlapping populations of interneurons (Table 1, Fig. 1, *D–F*).

Other cellular markers are commonly used to describe populations of interneurons. We therefore assessed immunoreactivity for the calcium-binding proteins calretinin (CR) and calbindin D_{28k} (CB) in EGFP-expressing interneurons using dual immunohistochemistry. CB immunoreactivity was found in nearly 33% and CR immunoreactivity in nearly 40% of EGFP-expressing interneurons (Table 1), findings that support the existence of subgroups of SST interneurons containing either of these calcium-binding proteins (see DISCUSSION).

TABLE 1. *Co-localization of GFP cells with cells expressing SST, PV, CB, and CR*

Labeling	Total Number of GFP Cells Counted	Total Number of GFP Cells Co-Localized	Percentage Co-Localization	Number of GIN Mice
SST	183*	181	99.0	3
PV	165	0	0.0	3
CB	110	38	33.4	3
CR	111	44	39.6	2

*Two GFP cells could not be unambiguously defined as co-localized with SST by fluorescence microscopy.

Electrophysiological classification of EGFP/SST-expressing neocortical interneurons

The aim of this study was to determine the degree of homogeneity in the population of EGFP-expressing interneurons in the GIN mouse somatosensory cortex. SST cells in rat frontal cortex have differing electrophysiological properties and are classified as either burst spiking (about 36%) or regular spiking (about 64%; Kawaguchi and Kubota 1996). It is not known whether the subpopulation in which EGFP is expressed represents a single subclass of SST interneurons or is functionally heterogeneous. In these experiments we asked whether insertion of EGFP into the *Gad1* gene resulted in labeling of a single electrophysiological subtype of SST interneuron.

Forty-six EGFP-expressing interneurons were electrophysiologically characterized according to the parameters described in METHODS above. Results are shown in Table 2 and further analyzed as parameters in unsupervised cluster analysis. R_{in} was eliminated on the basis of its strong correlations with other parameters (e.g., τ_m, sEPSC peak amplitude) because correlations between parameters unbalance the contributions of each parameter to the clustering algorithm, causing data points to skew toward the correlated parameters' axes in multidimensional space (Hair et al. 1998). R_{in} was also found post hoc not to be significantly different between cell groups (Table 2), thus providing no discrimination power. Spontaneous EPSC frequency, APHW, and accommodation of firing frequency were also eliminated, based on a heuristic process where multiple discriminant analysis is used to determine which parameters most strongly contribute to the separation of clusters (see METHODS). Cluster analysis, based on the remaining parameters, was applied to the sample of 46 EGFP-expressing interneurons.

This analysis yielded the dendrogram shown in Fig. 3*A*. Results from application of the Thorndike procedure (see METHODS) suggested that four clusters of neurons were present (Fig. 3*A*, *inset*), corresponding to branches 1, 2, 3, and 4. These results indicated that there is heterogeneity in the EGFP population of SST cells with respect to their electrophysiology. The electrophysiological characteristics of each group are examined in further detail below.

It was previously shown that there are differences in inhibitory transmission onto different interneuronal subtypes in the neocortex, explained in part by postsynaptic $GABA_A$-receptor–subunit composition in FS and LTS interneurons (Bacci et al. 2003b). In dentate gyrus there are also differences in the properties of inhibitory synaptic transmission from basket cells (BCs) onto granule cells versus onto other BCs (Bartos et al. 2001). However, little is known about the categorization of excitatory synapses onto interneurons in the neocortex. We therefore examined the EGFP-expressing interneurons in relation to their sEPSCs and other electrophysiological properties.

TABLE 2. *Electrophysiological properties of four types of EGFP-expressing cells*

	Group 1 (n = 17)	*Group 2 (n = 7)*	*Group 3 (n = 15)*	*Group 4 (n = 7)*
	Groups 1, 2, 3 ≫ 4; Groups 1, 2 > 3			
AHP shape, mV	1.6 ± 0.8	1.7 ± 1.0	0.8 ± 0.7	−3.6 ± 0.6
	Group 3 ≫ Groups 1, 2; Group 3 > Group 4			
Steady-state firing frequency, Hz	36.2 ± 9.6	28.8 ± 9.0	56.6 ± 17.5	37.2 ± 13.0
	Group 1 ≫ Group 4; Group 2 ≫ Groups 1, 3, 4			
Membrane time constant, ms	20.5 ± 6.5	31.4 ± 7.7	15.3 ± 3.4	9.8 ± 3.3
	Group 3 ≫ Groups 1, 2, 4			
Sag conductance, nS	1.7 ± 1.2	0.51 ± 0.72	3.9 ± 1.2	0.95 ± 1.0
	Group 1 ≫ Groups 2, 3			
sEPSC peak amplitude, pA	−18.1 ± 4.2	−31.1 ± 7.2	−25.7 ± 7.3	−25.1 ± 7.2
	Group 1 > Groups 2, 4			
sEPSC rise time, ms	1.9 ± 0.4	1.4 ± 0.4	1.6 ± 0.3	1.4 ± 0.1
	Group 1 ≫ Groups 2, 3, 4			
sEPSC decay time, ms	8.2 ± 1.4	5.0 ± 1.4	6.3 ± 1.5	4.8 ± 1.3
	Groups not significantly different (P > 0.1)			
Input resistance, MΩ	205 ± 30	224 ± 19	212 ± 27	213 ± 19
	Groups not significantly different (P > 0.1)			
Resting membrane potential, mV	−58.7 ± 3.6	−59.0 ± 2.7	−57.2 ± 3.3	−60.9 ± 3.8
	Groups not significantly different (P > 0.5)			
Series resistance MΩ	36.2 ± 9.6	28.8 ± 9.0	56.6 ± 17.5	37.2 ± 13.0
	Groups not significantly different (P > 0.1)			
f–I terminal slope Hz/nA	36.2 ± 9.6	28.8 ± 9.0	56.6 ± 17.5	37.2 ± 13.0

Values are means ± SD, *n,* number of cells; >, significantly greater with $P = 0.05$; ≫, significantly greater with $P = 0.01$. Statistically significant differences were determined using a Tukey post hoc means analysis after performing ANOVA. Electrophysiological parameters were measured as described in METHODS.

When firing and intrinsic membrane parameters were analyzed, three clusters were distinguished using the Thorndike procedure (Fig. 3*B*). All group 2 and group 4 cells remained clustered with their previously defined groups, indicating that they are mostly defined and distinguished from other groups by their firing and intrinsic membrane parameters. When just sEPSC parameters were analyzed, the Thorndike procedure suggested only two branches (Fig. 3*C*). In this case only group 1 cells were entirely separated, indicative of their segregation from other cells based mostly on sEPSC parameters. Cells from groups 3 and 4 are clustered together in one branch of this dendrogram, showing that they are similar with respect to their sEPSC properties, whereas their separation in the dendrogram of Fig. 3*B* indicates they differ with respect to their firing and intrinsic membrane properties. This helps the interpretation of the dendrogram in Fig. 3*A* and explains why cells from groups 3 and 4 are in the same secondary branch. However, it is important to note that all parameters are necessary to distinguish the four groups when considering the entire collection of EGFP-expressing interneurons.

The postsynaptic target of interneuronal axons is the best anatomical predictor of physiological cell type and is useful in deducing function within cortical circuits (de Lima and Morrison 1989; Deuchars and Thomson 1995; Tamas et al. 1997; Thomson et al. 1996; Xiang et al. 2002). Only gross proximal somatodendritic morphology could be visualized during whole cell recording (Fig. 2). Based on this limited anatomical information three anatomical categories of EGFP-expressing cells could be described (multipolar, bipolar, or unipolar; see METHODS) that were evenly distributed (Pearson's χ^2; $P > 0.1$) through all groups (Fig. 3*A*). From this we conclude that it is not possible to identify a cell's electrophysiological group membership by visual epifluorescent imaging before whole cell patch recording.

Electrophysiological characteristics of four EGFP-expressing cell groups

After classifying EGFP-expressing interneurons into four groups using cluster analysis, we were able to determine the groups' average electrophysiological characteristics. Representative traces from the electrophysiological analyses are shown in Fig. 4 and the data are summarized in Figs. 5 and 6 and Table 2.

Group 1 cells differ the most from other groups in terms of the sEPSC parameters; their sEPSC decay times are significantly slower than those of groups 2–4 (Figs. 4*D* and 6*C*; Table 2) and their rise times are significantly slower than those of groups 2 and 4 (Figs. 4*D* and 6*B*). There was also a small but significant reduction in sEPSC peak amplitude in cells of group 1 versus that of groups 2 and 3 (Figs. 4*D* and 6*A*; Table 2). The diversity seen in sEPSC characteristics is unlikely to result from differences in recording conditions because there was no significant difference in R_S between groups (Table 2). The membrane time constants of group 2 cells were significantly slower than those of all other groups (Figs. 4*A* and 5*C*; Table

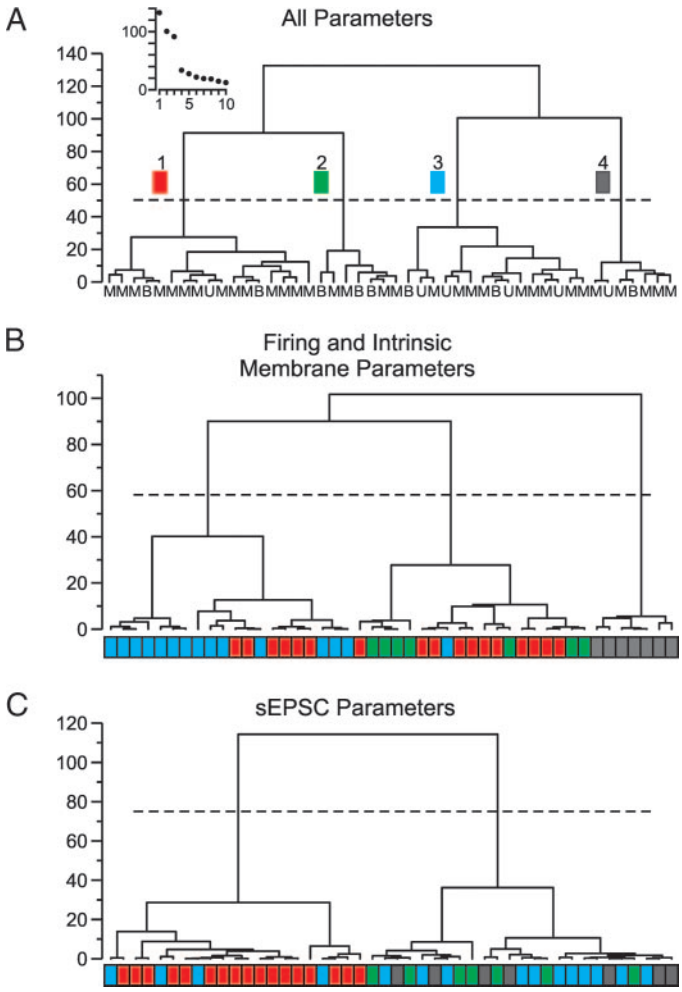

FIG. 3. Comparison of different cluster analysis strategies applied to EGFP neurons from GIN mice. Intersection of dendrogram branches with the *x*-axis represents individual neurons, whereas the *y*-axis represents the distance (squared Euclidean) between group centroids at each branch point (longer vertical lines indicate greater dissimilarity). Dashed lines indicate the number of groups as suggested by Thorndike's method (see METHODS). *A*: cluster analysis using noncorrelated, strongly discriminating parameters. *Inset*: using the Thorndike method, 4 groups are suggested in a scree plot; *x*-axis: first 10 clustering stages, *y*-axis: squared Euclidean distance between group centroids. Individual cells are also coded according to their membership to these 4 groups and indicated by colored boxes in *B* and *C*. Letters underneath indicate morphology of individual cells: bipolar (B), unipolar (U), and multipolar (M). *B*: cluster analysis based on firing properties [steady-state firing frequency and afterhyperpolarization (AHP) shape], membrane time constant, and H conductance. *C*: analysis using the spontaneous excitatory postsynaptic current (sEPSC) parameters of peak amplitude, rise time, and decay time.

2). Cells from group 3 had a significantly higher steady-state firing frequency than that of the other three groups (Figs. 4*B* and 5*B*; Table 2) and also had a significantly larger sag conductance than that of the other groups (Figs. 4*A4* and 5*D*; Table 2). The shape of the AP–AHP served to separate group 4 cells most clearly from other groups. Cells of groups 1, 2, and 3 all had AHPs with an easily discernible early and late component (Fig. 4*C*, *1–3*), whereas group 4 cells had either a less pronounced late component or did not have one at all (Figs. 4*C4* and 5*A*).

A method for determining group membership, without performing cluster analysis repeatedly with the addition of each newly encountered cell, would be useful if GIN mice are to be used for future physiological studies. Multiple discriminant analysis (MDA) performed on an adequately large population of cells previously classified by cluster analysis generates an algorithm that can be used to predict the group membership of a newly encountered cell, providing that information on all of the same parameters used in the cluster analysis is available for that neuron. Using MDA, we generated three discriminant functions that can be used to determine the group membership of future EGFP cells based on the parameters used for cluster analysis (Table 3). All three functions significantly contributed to the prediction of group membership (Wilk's lambda, $P < 0.01$), although the first two accounted for roughly 88% of the variance (function 1: 59.0%; function 2: 29.2%). Variables that correlate most highly with those two functions contribute the most to discrimination between groups. Although not indicated by the nonstandardized discriminant weights in Table 3, the contribution of variables to each discriminant function can be shown by MDA in a structure matrix (Table 4). The first discriminant function distinguished cells based mostly on the basis of AP–AHP shape. The second discriminant function is most strongly influenced by steady-state firing frequency and sag conductance. After the first two discriminant functions were applied, all of the cells were correctly classified. The third discriminant function, in addition to the first two, would allow the unambiguous separation of cells encountered in the future, especially those near the border between groups 1 and 2. The variables most strongly contributing to discriminant function 3 are membrane time constant, sEPSC peak amplitude, decay time, and rise time. This indicates that groups 1, 2, and 3 were similar to each other with respect to their firing and intrinsic properties and differed mostly in sEPSC properties because they are more stratified along the axis defined by discriminant function 2 (see following text and Fig. 7). To assess how well the discriminant functions work, and whether they work equally well for all groups, leave-one-out cross-validation was performed (Hair et al. 1998). The procedure of cross-validation is accomplished by classifying each cell by the functions derived from all cells but that cell. If the functions are not robust for determining group membership, omitting one cell will introduce errors in classification. We found that 100% of cross-validated cells were correctly classified.

The discriminant scores for the 46 cells of this study were determined for discriminant functions 1 and 2 and plotted (Fig. 7) to show the territorial map of each of the groups in a compressed two-dimensional representation of the seven parameters. With only the first and second function graphed, this plot provides good separation of all groups; however, there is a less distinct border between cells of groups 1 and 2 compared with the other borders.

DISCUSSION

EGFP interneurons are heterogeneous

SST interneurons in neocortex represent a heterogeneous group in terms of their electrophysiological (Kawaguchi and Kubota 1996) and molecular properties (Gonchar and Burkhalter 1997; Kubota and Kawaguchi 1994; Kubota et al. 1994). EGFP expression in SST interneurons of the GIN mouse allows easy visual identification of a subset of these GABAer-

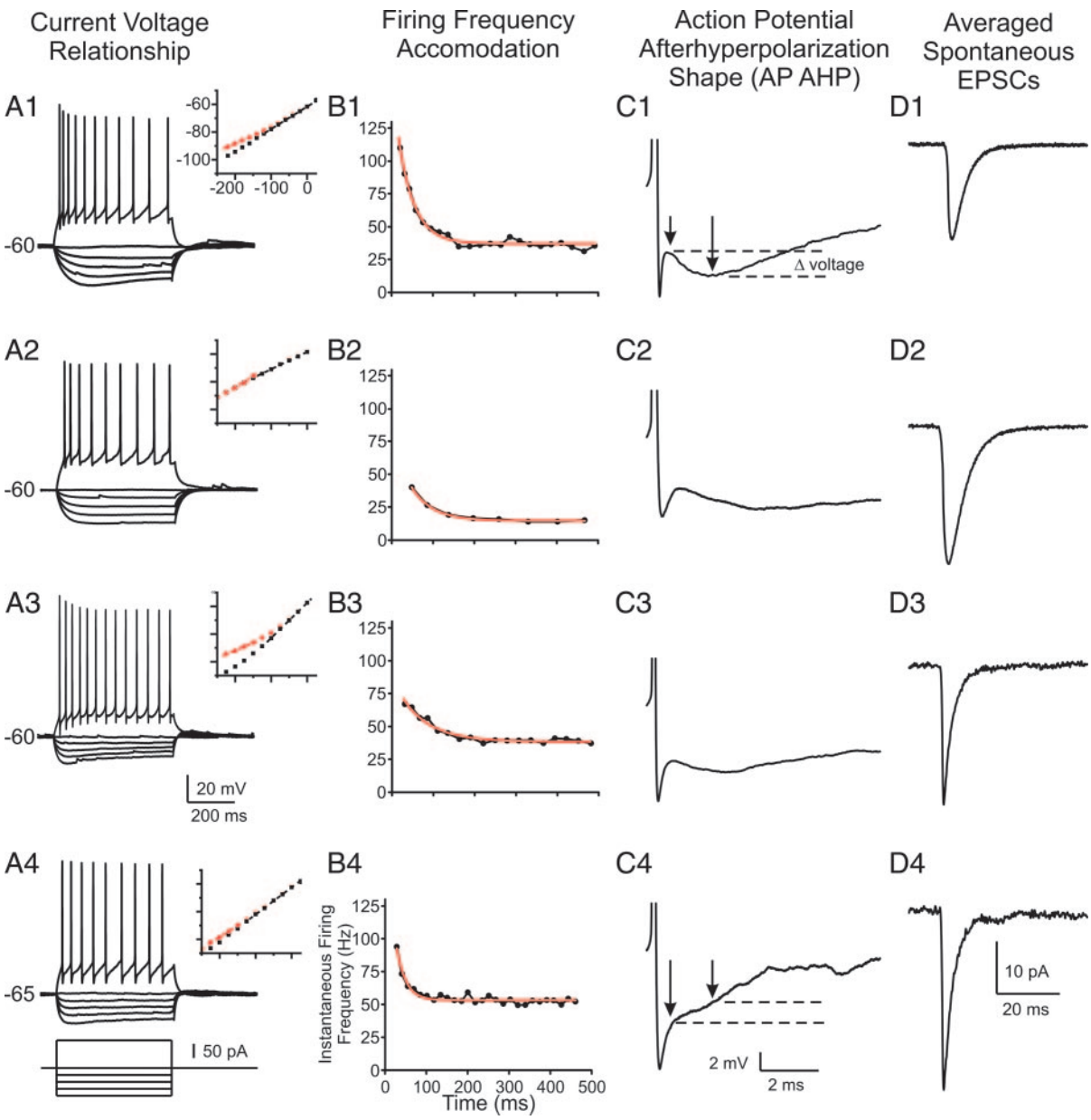

FIG. 4. Examples of electrophysiological characteristics of each of the 4 clusters of EGFP-expressing interneurons. Figures are organized as (letter)-group membership (e.g., A1, B1, C1, and D1 are from group 1.) *A*: responses to hyper- and depolarizing current steps recorded from cells at rest [V_R indicated to *left* of traces in millivolts (mV)]. *A*, *insets*: current–voltage plots indicating linear fits to determine membrane resistance near rest (black) or at end (red) of hyperpolarizing current pulses. Lines indicate the linear portions of plots used for fitting. *x*-axis: current pulse in picoamperes (pA); *y*-axis: V_m in mV. *B*: plots of action potential (AP) instantaneous firing frequency vs. time in response to a 125-pA depolarizing current step. Red lines are fitted curves using a single-exponential decay function. *C*: individual AP–AHPs recorded with current steps that depolarize cell just above threshold. Arrows indicate times at which membrane potential was used to determine AP–AHP shape; dashed lines indicate measure of AP–AHP shape. *D*: averaged traces of sEPSCs occurring in a 5-min recording window.

gic cells whose function in neocortex and hippocampus is incompletely understood. Insertion of the EGFP was performed in a manner that should have restricted it to a specific subset of GABAergic interneurons (Oliva Jr. et al. 2000). However, as is the case for SST interneurons in the cortex in general, EGFP-expressing interneurons of the GIN mouse also represent a heterogeneous group. Our data show that subgroups of these interneurons in sensorimotor cortex differ in their expression of calcium-binding proteins (Table 1), and at least four distinct cell populations can be identified electrophysiologically (Fig. 3). The implications of this functional heterogeneity are unknown, but potential consequences will be discussed in the following text.

Heterogeneity of cellular markers in EGFP-expressing neocortical interneurons

None of the EGFP-expressing interneurons sampled contained the calcium-binding protein PV (Table 1). In this respect they constitute a homogeneous population that resembles rat SST interneurons previously investigated (Kawaguchi and Kondo 2002; Kawaguchi and Kubota 1993, 1996). On the

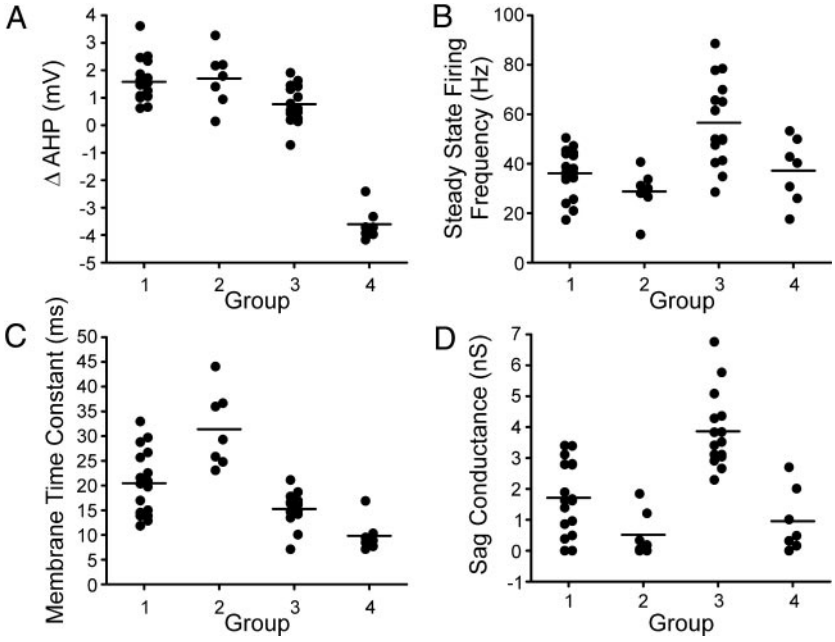

FIG. 5. Summary of intrinsic membrane and firing properties for the 4 groups of neurons determined by cluster analysis. Data for all cells in each group are plotted. Mean of each group for each parameter is indicated by the horizontal line. Refer to Table 1 for statistical analysis of differences.

other hand, the calcium-binding protein calbindin D_{28k} (CB), which is coexpressed in nearly 85% of all rat neocortical SST interneurons (Gonchar and Burkhalter 1997; Kubota et al. 1994; Rogers 1992), was present in only about 33% of EGFP-expressing interneurons (Table 1). The possibility that the proportion of CB-containing interneurons is also reduced in the non-EGFP group of SST interneurons in the GIN mouse has not been eliminated, but seems unlikely in light of the data from rat (references above).

Our results show that calretinin (CR) immunoreactivity is present in nearly 40% of EGFP-expressing interneurons in the GIN mouse sensorimotor cortex (Table 1). This finding conflicts with previous reports indicating that CR is not coexpressed with SST in frontal and visual areas of rat neocortex (Gonchar and Burkhalter 1997; Kubota et al. 1994). However, in the rat somatosensory cortex, CR mRNA was found in 16% of cells containing SST mRNA (Cauli et al. 1997; Wang et al. 2004). A reason for these discrepancies could be species differences between mice and rats. It is also possible that various cortical areas show differences in CR coexpression with SST. A variety of chemical markers, such as CB and tachykinin, show area-specific localizations (DeFelipe et al. 1990; Hof et al. 1995; Jones et al. 1995). The density of CR immunoreactivity is also significantly different between distinct areas of primate visual cortex (DeFelipe et al. 1999) and between prefrontal, somatosensory, motor, and visual primate cortex (Elston and Gonzalez-Albo 2003). Our finding of CB and CR immunoreactivity in EGFP-expressing interneurons of the neocortex contrasts with the observations of Oliva Jr. et al. (2000), who found no immunoreactivity for CB or CR in hippocampal EGFP-expressing interneurons.

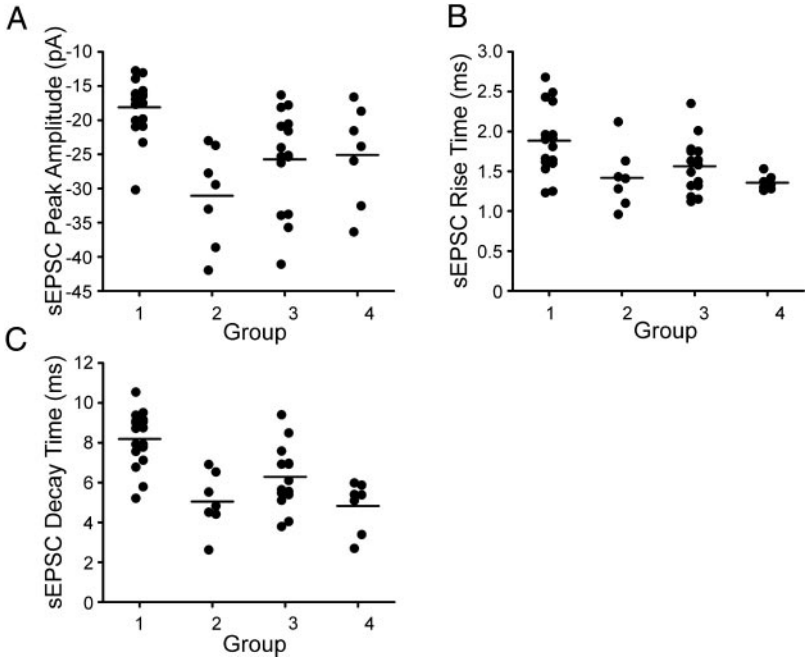

FIG. 6. Summary of the sEPSC properties for the 4 groups of neurons determined by cluster analysis. Data for all cells in each group are plotted. Mean of each group for each parameter is indicated by the horizontal line. Refer to Table 1 for statistical analysis of differences.

TABLE 3. *Discriminant function weights for determining group membership*

		Variable Discriminant Weights						
						sEPSC		
Discriminant Function	Intercept	AP–AHP shape	SSFF	τ_m	G_S	Amplitude	RT	DT
1	−1.59	1.38	0.00	−0.04	0.01	0.01	0.13	0.43
2	−0.98	0.41	0.07	−0.15	0.56	−0.04	0.22	−0.26
3	0.34	−0.29	−0.01	−0.08	0.01	−0.07	1.02	0.39

Abbreviations are explained in METHODS; weights are unstandardized.

The function of various calcium-binding proteins in EGFP- or non–EGFP-expressing cells is not known. However, differences between subgroups of interneurons could reflect differences in Ca^{2+} buffering capacity that regulate the spread of dendritic Ca^{2+} signals (Goldberg and Yuste 2005) and Ca^{2+}-dependent processes such as activation of K^+ channels.

Electrophysiological heterogeneity of EGFP-expressing interneurons

There are a great number of variables that might be correlative and/or causative for the electrophysiologically determined subtypes of EGFP-expressing interneurons in the GIN mouse, including a variety of ion channels that determine the spiking phenotype of a given neuron, as well as receptor subtypes and transporters, for instance. The heterogeneity in expression of channel proteins is likely just one of the factors responsible for defining the functional phenotype of this diverse population of cells. Layer II/III rat SST interneurons have axonal projections predominantly onto dendrites or dendritic tufts of pyramidal cells (Markram et al. 2004) and may regulate dendritic excitability and the efficacy of excitatory inputs. However, in addition to this spatial regulation, the intrinsic spiking properties of interneurons likely determine the timing and intensity of their postsynaptic effects (Cauli et al. 1997; Kawaguchi and Kubota 1997). It is then possible that the differences in firing and sEPSC characteristics observed between cell groups in the present study represent further functional differentiation in the subgroup of EGFP-expressing SST interneurons.

AP FIRING HETEROGENEITY. In the rat, SST interneurons are electrophysiologically diverse and include bursting and regular spiking phenotypes (Kawaguchi and Kubota 1996). The firing properties of BSNP cells are similar to those of the interneurons of groups 1–3 in this study; that is, these cells showed a pronounced slow AHP component. In contrast, RSNP cells were more similar to our group 4 cells, showing a much smaller or nonexistent slow AHP component. In previously reported cluster analysis of cortical interneurons using parameters including molecular and electrophysiological markers, only one population of regular spiking nonpyramidal (RSNP) SST interneurons was found (Cauli et al. 2000). However, the authors restricted the population of cells they investigated to fusiform (bipolar) interneurons. The majority of EGFP-expressing cells in this present study were not bipolar, possibly indicating that the bipolar cells studied earlier (Cauli et al. 2000) represent a non–EGFP-expressing population of SST interneurons. In contrast to the results of Cauli and colleagues (2000), we did not find any correlation between gross cell morphology (shape of somata and numbers of proximal dendritic branches) and electrophysiological classification among EGFP/SST cells in the GIN mouse. Other investigators have also noted a lack of phenotypic morphological–electrophysiological correlation in rat hippocampal interneurons (Parra et al. 1998). However, axonal arbors and fine dendritic branches of EGFP-expressing interneurons are not easily seen within in vitro slices, and additional anatomical studies will be required to assess more extensively their morphology and any correlations with electrophysiological groups.

In addition to the differences in APs between groups discussed above, we find that there is further heterogeneity between groups 1–3 based on steady-state firing frequency (SSFF). Group 3 cells are able to sustain a much higher rate of AP firing, perhaps allowing them to maintain tonic GABA and/or SST release.

The differences in SSFF and AP–AHP indices between groups in this study (Table 2 and Fig. 5, *A* and *B*) likely represent variable expression of K^+ channel subunits in EGFP-expressing interneurons. Kv3 subunits, responsible for delayed rectifier currents, are thought to enable fast sustained firing (Erisir et al. 1999; Rudy and McBain 2001) and are expressed differentially among rat neocortical interneurons. Whereas

TABLE 4. *Structure matrix coefficients*

	Structure Coefficients						
					sEPSC		
Discriminant Function	AP–AHP shape	SSFF	τ_m	G_S	Amplitude	RT	DT
1	0.79*	0.001	0.22	0.09	0.12	0.17	0.27
2	−0.04	0.40*	−0.35	0.56*	−0.03	−0.03	−0.01
3	−0.55	−0.02	−0.55*	0.00	0.51*	0.26*	0.44*

The structure coefficients indicate the simple Pearsonian correlations between parameters and the discriminant functions. An asterisk (*) indicates the largest absolute correlation between each variable and any discriminant function; that is, this variable will stratify or segregate the cells most along this function's axis relative to the other functions.

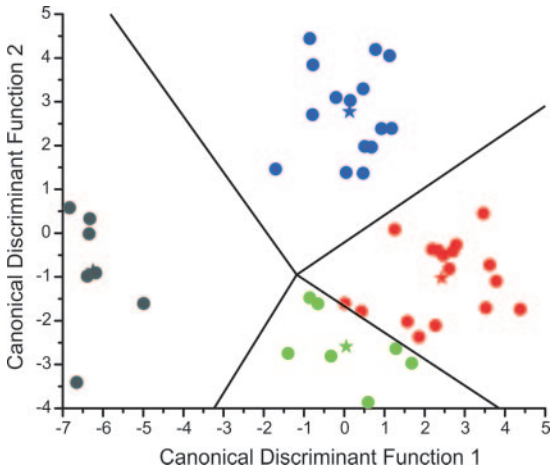

FIG. 7. Territorial map generated with multiple discriminant analysis showing the distribution of cells used in this study. Only the first 2 of 3 discriminant functions are used here. These can be used to predict group membership of newly encountered cells by plotting their discriminant scores and determining the territory into which they fall. Lines indicate critical cutting scores and stars indicate group centroids. Colors are the same as for Fig. 3.

Kv3.1 expression is restricted to FS PV positive interneurons, Kv3.2 expression is also found in a subset of non-FS SST interneurons (Chow et al. 1999). However, Kv3.2 overlap with SST expression in rats is restricted to deeper layers (V–VI; Chow et al. 1999), whereas EGFP-expressing interneurons in the GIN mouse are located mostly in layers II and III of neocortex and not in layers V–VI (Oliva Jr. et al. 2000). This may indicate segregation between EGFP-expressing SST interneurons and SST interneurons that do not express EGFP in the GIN mouse.

Ca^{2+}-activated K^+ currents modulate the AP time course and the repetitive firing properties of neurons. Fast AHPs have been partially attributed to currents through Ca^{2+}- and voltage-activated NK channels (I_C), whereas slow AHPs are related to Ca^{2+}-activated SK channel currents (I_{AHP}; Bond et al. 1999; Sah and Faber 2002). The current arising from activation of BK channels has an activation rate consistent with the AP–AHPs seen in this study and could be responsible in part for the AP repolarization, as well as the early component of the AP–AHP seen in all groups. An apamin-sensitive current carried by SK2 and SK3 channels activates rapidly after an AP and has a decay time constant of about 150 ms (Bond et al. 1999). This current may underlie the slow AP–AHP component seen in groups 1, 2, and 3 (Figs. 4*C*, *1–3* and 5*A*).

HETEROGENEITY OF PROPERTIES INFLUENCING SYNAPTIC INTEGRATION. Along with the differences in active response to inputs, EGFP-expressing cells also exhibit heterogeneity in properties that can passively shape a cell's postsynaptic responses. The large sag conductance seen in group 3 (Figs. 4*A*, *1–2* and 5*D*) may facilitate the generation of rebound AP bursts in response to inhibitory inputs. The back-propagation of such bursts into dendrites (Kaiser et al. 2004) may affect postsynaptic Ca^{2+} dynamics and responses to excitatory inputs.

There are also differences in their membrane time constants in EGFP-expressing interneurons, with group 4 cells having membrane time constants significantly faster than those of groups 1 and 2 (Figs. 4*A4* and 5*C*). This may allow more faithful propagation of distal inputs to the soma, allowing better temporal segregation of inputs (see also discussion of sEPSC properties below).

HETEROGENEITY OF SPONTANEOUS EPSCS. As is the case for α-amino-3-hydroxy-5-methyl-4-isoxazolepropionic acid (AMPA)–receptor-mediated EPSCs in rat RSNP neurons in the rat (Angulo et al. 1997), sEPSC kinetics in EGFP-expressing interneurons in this study were also variable. Variations in the locations of synapses and/or the geometry of their dendritic trees (Rall 1962) along with the structure of the synapse (Cathala et al. 2005) could underlie the faster rise and decay times of the cells of groups 2, 3, and 4, versus those in group 1. Faster kinetics would allow more restricted temporal correlation of incoming signals (e.g., presynaptic APs), similar to that suggested for the faster EPSP kinetics of FS neurons, relative to those seen in RSNP interneurons (Angulo et al. 1997). On the other hand, a slow synaptic conductance would maximize the temporal summation of EPSCs, allowing the preferential activation of group 1 cells, over cells of groups 2, 3, and 4, by bursts in presynaptic pyramidal neurons (Kaiser et al. 2004; Kozloski et al. 2001; Markram et al. 1998).

Cluster analysis was used by Krimer et al. (2005) to classify neurons in layer 2/3 of monkey dorsolateral prefrontal cortical slices on the basis of electrophysiological parameters. These authors found that all layer 2/3 cells could be classified into three distinct groups consisting of regular spiking (RS), intermediate spiking (IS), and fast spiking (FS) cells. They found further heterogeneity within the groups based on morphological phenotype. Based on the physiological and morphological descriptions of the cells in Krimer et al. (2005), it is likely that the EGFP-expressing interneurons of the GIN mouse analyzed here correspond to subgroups of cells contained within their RS and IS cell groups.

Putative role of EGFP-expressing interneurons in normal and pathological cortical function

SST interneurons in the hippocampus and dentate gyrus are selectively vulnerable to injury in epilepsy (Buckmaster and Dudek 1997; Buckmaster and Jongen-Relo 1999; Kobayashi and Buckmaster 2003; Sloviter 1987, 1991; Sloviter and Lowenstein 1992) and traumatic brain injury (Lowenstein et al. 1992), and they are also affected by Alzheimer's disease in the cortex and hippocampus (Davies et al. 1980; Grouselle et al. 1998; Roberts et al. 1985; Van Uden et al. 1999). If the GIN mouse or other murine strains with either EGFP- or YFP-labeled neuronal subtypes are to be used to study anatomical or physiological effects of such disease processes, it will be important to take into account heterogeneity within the labeled population; that is, particular subclasses may be vulnerable to injury, whereas others are resistant. Our results show that subgroups of neurons for such studies can be identified using cluster analysis and group membership for single "unknown" neurons within a subpopulation can easily be predicted using multiple discriminant analysis.

ACKNOWLEDGMENTS

We thank I. Parada for invaluable assistance.

GRANTS

This work was supported by National Institute of Neurological Disorders and Stroke Grants NS-12151, NS-039579, and NS-02780.

REFERENCES

Angulo MC, Lambolez B, Audinat E, Hestrin S, and Rossier J. Subunit composition, kinetic, and permeation properties of AMPA receptors in single neocortical nonpyramidal cells. *J Neurosci* 17: 6685–6696, 1997.

Bacci A, Huguenard JR, and Prince DA. Functional autaptic neurotransmission in fast-spiking interneurons: a novel form of feedback inhibition in the neocortex. *J Neurosci* 23: 859–866, 2003.

Bacci A, Rudolph U, Huguenard JR, and Prince DA. Major differences in inhibitory synaptic transmission onto two neocortical interneuron subclasses. *J Neurosci* 23: 9664–9674, 2003.

Bartos M, Vida I, Frotscher M, Geiger JR, and Jonas P. Rapid signaling at inhibitory synapses in a dentate gyrus interneuron network. *J Neurosci* 21: 2687–2698, 2001.

Bond CT, Maylie J, and Adelman JP. Small-conductance calcium-activated potassium channels. *Ann NY Acad Sci* 868: 370–378, 1999.

Buckmaster PS and Dudek FE. Neuron loss, granule cell axon reorganization, and functional changes in the dentate gyrus of epileptic kainate-treated rats. *J Comp Neurol* 385: 385–404, 1997.

Buckmaster PS and Jongen-Relo AL. Highly specific neuron loss preserves lateral inhibitory circuits in the dentate gyrus of kainate-induced epileptic rats. *J Neurosci* 19: 9519–9529, 1999.

Cathala L, Holderith NB, Nusser Z, DiGregorio DA, and Cull-Candy SG. Changes in synaptic structure underlie the developmental speeding of AMPA receptor-mediated EPSCs. *Nat Neurosci* 8: 1310–1318, 2005.

Cauli B, Audinat E, Lambolez B, Angulo MC, Ropert N, Tsuzuki K, Hestrin S, and Rossier J. Molecular and physiological diversity of cortical nonpyramidal cells. *J Neurosci* 17: 3894–3906, 1997.

Cauli B, Porter JT, Tsuzuki K, Lambolez B, Rossier J, Quenet B, and Audinat E. Classification of fusiform neocortical interneurons based on unsupervised clustering. *Proc Natl Acad Sci USA* 97: 6144–6149, 2000.

Chow A, Erisir A, Farb C, Nadal MS, Ozaita A, Lau D, Welker E, and Rudy B. K(+) channel expression distinguishes subpopulations of parvalbumin- and somatostatin-containing neocortical interneurons. *J Neurosci* 19: 9332–9345, 1999.

Davies P, Katzman R, and Terry RD. Reduced somatostatin-like immunoreactivity in cerebral cortex from cases of Alzheimer disease and Alzheimer senile dementa. *Nature* 288: 279–280, 1980.

DeFelipe J. Neocortical neuronal diversity: chemical heterogeneity revealed by colocalization studies of classic neurotransmitters, neuropeptides, calcium-binding proteins, and cell surface molecules. *Cereb Cortex* 3: 273–289, 1993.

DeFelipe J. Types of neurons, synaptic connections and chemical characteristics of cells immunoreactive for calbindin-D28K, parvalbumin and calretinin in the neocortex. *J Chem Neuroanat* 14: 1–19, 1997.

DeFelipe J. Cortical interneurons: from Cajal to 2001. *Prog Brain Res* 136: 215–238, 2002.

DeFelipe J and Farinas I. The pyramidal neuron of the cerebral cortex: morphological and chemical characteristics of the synaptic inputs. *Prog Neurobiol* 39: 563–607, 1992.

DeFelipe J, Gonzalez-Albo MC, Del Rio MR, and Elston GN. Distribution and patterns of connectivity of interneurons containing calbindin, calretinin, and parvalbumin in visual areas of the occipital and temporal lobes of the macaque monkey. *J Comp Neurol* 412: 515–526, 1999.

DeFelipe J, Hendry SH, Hashikawa T, Molinari M, and Jones EG. A microcolumnar structure of monkey cerebral cortex revealed by immunocytochemical studies of double bouquet cell axons. *Neuroscience* 37: 655–673, 1990.

de Lima AD and Morrison JH. Ultrastructural analysis of somatostatin-immunoreactive neurons and synapses in the temporal and occipital cortex of the macaque monkey. *J Comp Neurol* 283: 212–227, 1989.

Deuchars J and Thomson AM. Innervation of burst firing spiny interneurons by pyramidal cells in deep layers of rat somatomotor cortex: paired intracellular recordings with biocytin filling. *Neuroscience* 69: 739–755, 1995.

Elston GN and Gonzalez-Albo MC. Parvalbumin-, calbindin-, and calretinin-immunoreactive neurons in the prefrontal cortex of the owl monkey (*Aotus trivirgatus*): a standardized quantitative comparison with sensory and motor areas. *Brain Behav Evol* 62: 19–30, 2003.

Erisir A, Lau D, Rudy B, and Leonard CS. Function of specific K(+) channels in sustained high-frequency firing of fast-spiking neocortical interneurons. *J Neurophysiol* 82: 2476–2489, 1999.

Franklin KBJ and Paxinos G. *The Mouse Brain in Stereotaxic Coordinates.* San Diego, CA: Academic Press, 1997.

Goldberg JH and Yuste R. Space matters: local and global dendritic Ca^{2+} compartmentalization in cortical interneurons. *Trends Neurosci* 28: 158–167, 2005.

Gonchar Y and Burkhalter A. Three distinct families of GABAergic neurons in rat visual cortex. *Cereb Cortex* 7: 347–358, 1997.

Grouselle D, Winsky-Sommerer R, David JP, Delacourte A, Dournaud P, and Epelbaum J. Loss of somatostatin-like immunoreactivity in the frontal cortex of Alzheimer patients carrying the apolipoprotein epsilon 4 allele. *Neurosci Lett* 255: 21–24, 1998.

Gupta A, Wang Y, and Markram H. Organizing principles for a diversity of GABAergic interneurons and synapses in the neocortex. *Science* 287: 273–278, 2000.

Hair JF, Anderson RE, Tatham RL, and Black WC. *Multivariate Data Analysis.* Upper Saddle River, NJ: Prentice Hall, 1998.

Hof PR, Nimchinsky EA, and Morrison JH. Neurochemical phenotype of corticocortical connections in the macaque monkey: quantitative analysis of a subset of neurofilament protein-immunoreactive projection neurons in frontal, parietal, temporal, and cingulate cortices. *J Comp Neurol* 362: 109–133, 1995.

Jones EG, Dell'Anna ME, Molinari M, Rausell E, and Hashikawa T. Subdivisions of macaque monkey auditory cortex revealed by calcium-binding protein immunoreactivity. *J Comp Neurol* 362: 153–170, 1995.

Kaiser KM, Lubke J, Zilberter Y, and Sakmann B. Postsynaptic calcium influx at single synaptic contacts between pyramidal neurons and bitufted interneurons in layer 2/3 of rat neocortex is enhanced by backpropagating action potentials. *J Neurosci* 24: 1319–1329, 2004.

Kawaguchi Y and Kondo S. Parvalbumin, somatostatin and cholecystokinin as chemical markers for specific GABAergic interneuron types in the rat frontal cortex. *J Neurocytol* 31: 277–287, 2002.

Kawaguchi Y and Kubota Y. Correlation of physiological subgroupings of nonpyramidal cells with parvalbumin- and calbindinD28k-immunoreactive neurons in layer V of rat frontal cortex. *J Neurophysiol* 70: 387–396, 1993.

Kawaguchi Y and Kubota Y. Physiological and morphological identification of somatostatin- or vasoactive intestinal polypeptide-containing cells among GABAergic cell subtypes in rat frontal cortex. *J Neurosci* 16: 2701–2715, 1996.

Kawaguchi Y and Kubota Y. GABAergic cell subtypes and their synaptic connections in rat frontal cortex. *Cereb Cortex* 7: 476–486, 1997.

Kobayashi M and Buckmaster PS. Reduced inhibition of dentate granule cells in a model of temporal lobe epilepsy. *J Neurosci* 23: 2440–2452, 2003.

Kozloski J, Hamzei-Sichani F, and Yuste R. Stereotyped position of local synaptic targets in neocortex. *Science* 293: 868–872, 2001.

Krimer LS, Zaitsev AV, Czanner G, Kroner S, Gonzalez-Burgos G, Povysheva NV, Iyengar S, Barrionuevo G, and Lewis DA. Cluster analysis-based physiological classification and morphological properties of inhibitory neurons in layers 2–3 of monkey dorsolateral prefrontal cortex. *J Neurophysiol* 94: 3009–3022, 2005.

Kubota Y, Hattori R, and Yui Y. Three distinct subpopulations of GABAergic neurons in rat frontal agranular cortex. *Brain Res* 649: 159–173, 1994.

Kubota Y and Kawaguchi Y. Three classes of GABAergic interneurons in neocortex and neostriatum. *Jpn J Physiol* 44, *Suppl*. 2: S145–S148, 1994.

Letinic K, Zoncu R, and Rakic P. Origin of GABAergic neurons in the human neocortex. *Nature* 417: 645–649, 2002.

Li H and Prince DA. Synaptic activity in chronically injured, epileptogenic sensory-motor neocortex. *J Neurophysiol* 88: 2–12, 2002.

Lowenstein DH, Thomas MJ, Smith DH, and McIntosh TK. Selective vulnerability of dentate hilar neurons following traumatic brain injury: a potential mechanistic link between head trauma and disorders of the hippocampus. *J Neurosci* 12: 4846–4853, 1992.

Maccaferri G and Lacaille JC. Interneuron diversity series: hippocampal interneuron classifications—making things as simple as possible, not simpler. *Trends Neurosci* 26: 564–571, 2003.

Markram H, Toledo-Rodriguez M, Wang Y, Gupta A, Silberberg G, and Wu C. Interneurons of the neocortical inhibitory system. *Nat Rev Neurosci* 5: 793–807, 2004.

Markram H, Wang Y, and Tsodyks M. Differential signaling via the same axon of neocortical pyramidal neurons. *Proc Natl Acad Sci USA* 95: 5323–5328, 1998.

Mott DD and Dingledine R. Interneuron diversity series: interneuron research—challenges and strategies. *Trends Neurosci* 26: 484–488, 2003.

Oliva AA Jr, Jiang M, Lam T, Smith KL, and Swann JW. Novel hippocampal interneuronal subtypes identified using transgenic mice that express green fluorescent protein in GABAergic interneurons. *J Neurosci* 20: 3354–3368, 2000.

Parra P, Gulyas AI, and Miles R. How many subtypes of inhibitory cells in the hippocampus? *Neuron* 20: 983–993, 1998.

Peters A and Sethares C. Organization of pyramidal neurons in area 17 of monkey visual cortex. *J Comp Neurol* 306: 1–23, 1991.

Rall W. Theory of physiological properties of dendrites. *Ann NY Acad Sci* 96: 1071–1092, 1962.

Roberts GW, Crow TJ, and Polak JM. Location of neuronal tangles in somatostatin neurones in Alzheimer's disease. *Nature* 314: 92–94, 1985.

Rogers JH. Immunohistochemical markers in rat cortex: co-localization of calretinin and calbindin-D28k with neuropeptides and GABA. *Brain Res* 587: 147–157, 1992.

Rudy B and McBain CJ. Kv3 channels: voltage-gated K^+ channels designed for high-frequency repetitive firing. *Trends Neurosci* 24: 517–526, 2001.

Sah P and Faber ES. Channels underlying neuronal calcium-activated potassium currents. *Prog Neurobiol* 66: 345–353, 2002.

Sloviter RS. Decreased hippocampal inhibition and a selective loss of interneurons in experimental epilepsy. *Science* 235: 73–76, 1987.

Sloviter RS. Permanently altered hippocampal structure, excitability, and inhibition after experimental status epilepticus in the rat: the "dormant basket cell" hypothesis and its possible relevance to temporal lobe epilepsy. *Hippocampus* 1: 41–66, 1991.

Sloviter RS and Lowenstein DH. Heat shock protein expression in vulnerable cells of the rat hippocampus as an indicator of excitation-induced neuronal stress. *J Neurosci* 12: 3004–3009, 1992.

Somogyi P, Tamas G, Lujan R, and Buhl EH. Salient features of synaptic organisation in the cerebral cortex. *Brain Res Brain Res Rev* 26: 113–135, 1998.

Tamas G, Buhl EH, and Somogyi P. Fast IPSPs elicited via multiple synaptic release sites by different types of GABAergic neurone in the cat visual cortex. *J Physiol* 500: 715–738, 1997.

Thomson AM and Deuchars J. Temporal and spatial properties of local circuits in neocortex. *Trends Neurosci* 17: 119–126, 1994.

Thomson AM, West DC, Hahn J, and Deuchars J. Single axon IPSPs elicited in pyramidal cells by three classes of interneurones in slices of rat neocortex. *J Physiol* 496: 81–102, 1996.

Thorndike RL. Who belongs in the family? *Psychometrika* 18: 267–276, 1953.

Van Uden E, Veinbergs I, Mallory M, Orlando R, and Masliah E. A novel role for receptor-associated protein in somatostatin modulation: implications for Alzheimer's disease. *Neuroscience* 88: 687–700, 1999.

Wang Y, Toledo-Rodriguez M, Gupta A, Wu C, Silberberg G, Luo J, and Markram H. Anatomical, physiological and molecular properties of Martinotti cells in the somatosensory cortex of the juvenile rat. *J Physiol* 561: 65–90, 2004.

Ward JH Jr. Hierarchical grouping to optimize an objective function. *J Am Stat Assoc* 58: 236–234, 1963.

Xiang Z, Huguenard JR, and Prince DA. Synaptic inhibition of pyramidal cells evoked by different interneuronal subtypes in layer V of rat visual cortex. *J Neurophysiol* 88: 740–750, 2002.